A review of heat treatments on improving the quality and residual stresses of the Ti–6Al–4V parts produced by additive manufacturing

metals

MDPI

Review

A Review of Heat Treatments on Improving the Quality and Residual Stresses of the Ti–6Al–4V Parts Produced by Additive Manufacturing

Óscar Teixeira [1], Francisco J. G. Silva [1,*], Luís P. Ferreira [1] and Eleonora Atzeni [2]

[1] ISEP—School of Engineering, Polytechnic of Porto, Rua Dr. António Bernardino de Almeida, 431, 4249-015 Porto, Portugal; oscarfrmteixeira96@gmail.com (Ó.T.); luispintoferreira@eu.ipp.pt (L.P.F.)

[2] Department of Management and Production Engineering (DIGEP), Politecnico di Torino, Corso Duca degli Abruzzi, 24, 10129 Torino (TO), Italy; eleonora.atzeni@polito.it

* Correspondence: fgs@isep.ipp.pt; Tel.: +351-228-340-500

Received: 4 July 2020; Accepted: 24 July 2020; Published: 27 July 2020

Abstract: Additive manufacturing (AM) can be seen as a disruptive process that builds complex components layer upon layer. Two of its distinct technologies are Selective Laser Melting (SLM) and Electron Beam Melting (EBM), which are powder bed fusion processes that create metallic parts with the aid of a beam source. One of the most studied and manufactured superalloys in metal AM is the Ti–6Al–4V, which can be applied in the aerospace field due to its low density and high melting point, and in the biomedical area owing to its high corrosion resistance and excellent biocompatibility when in contact with tissues or bones of the human body. The research novelty of this work is the aggregation of all kinds of data from the last 20 years of investigation about Ti–6Al–4V parts manufactured via SLM and EBM, namely information related to residual stresses (RS), as well as the influence played by different heat treatments in reducing porosity and increasing mechanical properties. Throughout the report, it can be seen that the expected microstructure of the Ti–6Al–4V alloy is different in both manufacturing processes, mainly due to the distinct cooling rates. However, heat treatments can modify the microstructure, reduce RS, and increase the ductility, fatigue life, and hardness of the components. Furthermore, distinct post-treatments can induce compressive RS on the part's surface, consequently enhancing the fatigue life.

Keywords: additive manufacturing; metal powder bed fusion; selective laser melting; electron beam melting; Ti–6Al–4V; residual stresses; heat treatments; microstructure

1. Introduction

Additive manufacturing (AM), also known by many as three-dimensional printing (3DP), was born in 1981 through Hideo Kodama [1] and can be described, according to the International Organization for Standardization (ISO) 52900-15 standard [2], as a manufacturing process that creates 3D objects from scratch, typically layer after layer. As a matter of fact, this technology can be seen as a disruptive one, as it completely changed the creation of parts through the addition of material instead of the common subtraction of it, something that is characteristic of subtractive manufacturing [3]. Furthermore, it can be classified as a sustainable process as it enables the production of complex geometry components with minimal waste of material [4]. One of the process categories associated with this new manufacturing process is called Powder Bed Fusion, which agglomerates three distinct technologies, namely Selective Laser Sintering (SLS), Selective Laser Melting (SLM), and Electron Beam Melting (EBM) (Figure 1) [5]. However, if one desires to produce exclusively metal components, then it must employ the last two mentioned technologies. Thus, from now on, this paper review will solely focus on SLM and EBM, as they are seen as metal Powder Bed Fusion technologies.

In fact, SLM appeared in 1996 through Wilhelm Meiners, Konrad Wissenbach, and Andres Gasser [6], and it is a process that must be done in a closed chamber surrounded by an inert gas, such as argon or nitrogen, to avoid oxidation of the material after melting, remove spatter, metal vapor, and plasma plumes [7–10]. In addition, the parts are usually connected to a substrate plate by support structures, in order to reduce deformations when manufacturing. The operating method is done by firstly heating up the building platform in order to reduce deformations caused by temperature differences (only on some machines); then, the powder cartridge rises, thanks to an actuator, and dispenses a predefined amount of powder. After that, the leveling roller/blade creates a uniform layer of powder on the construction platform and places the substrate excess in another cartridge opposite the first one, after which a high-energy density laser melts the powder, forming a melt pool of approximately 100 µm width [11]. Finally, the construction platform lowers according to the thickness of each layer, which usually varies between 20 and 100 µm depending on the material, and the process is repeated until the final part is completed [12].

ARCAM was founded in 1997 and is the only enterprise that manufactures EBM machines, as they own the patent [13]. This technology uses accelerated electrons in the order of 0.1 to 0.4 times the speed of light [14] as a beam source, and the process is done in a vacuum chamber [15]. Furthermore, the additive manufacturing steps are the same as the SLM technology; however, the temperature of the build chamber is much higher (500–800 °C) [16–19]. Hence, one should expect fewer residual stresses (RS) because of the lower temperature gradient during manufacturing (Tmelt–Tambient). In addition, the typical layer thickness of the parts is between 50 and 200 µm, due to the deeper penetration and higher energy of the beam, making the manufacturing process quicker than SLM [16].

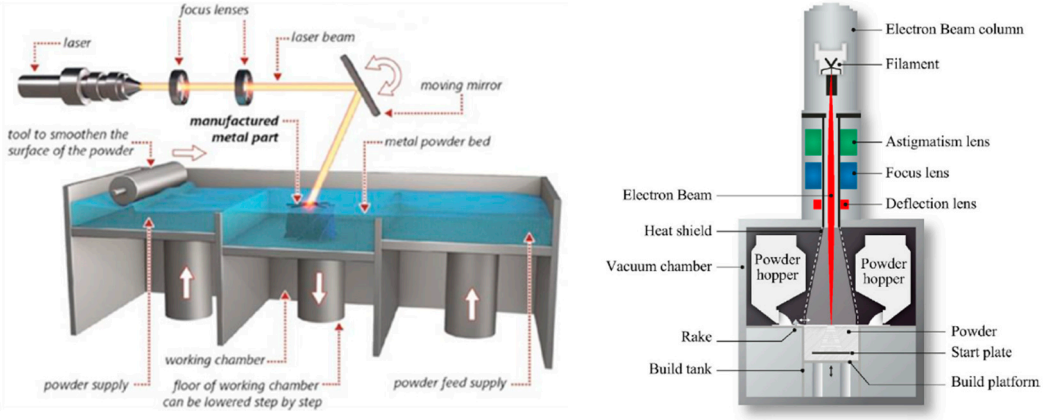

Figure 1. Main components of (**a**) Selective Laser Melting (SLM) machine, (**b**) Electron Beam Melting (EBM) machine. Adapted from [20], under CC BY 4.0. Original sources: (**a**) EMPA, (**b**) ARCAM.

Titanium alloys have been receiving special attention from the aerospace industry, thanks to the low density and the high melting point of this material (around 1650 °C) [21]. In other words, several companies turn to titanium when they need a light component that is capable of safely supporting high loads and/or when working temperatures are high [22]. In addition, it has also a high corrosion resistance [23–25], and it is often used in medical implants due to its excellent biocompatibility when in contact with tissues or bones of the human body [26]. Note that this material is quite difficult and expensive to machine, so its use and diffusion in AM is of great interest [27,28]. In fact, the titanium alloy most studied by the scientific community and used to manufacture final components is Ti–6Al–4V (UNS R56400) [29]. The crystalline structure of this alloy is composed of a compact hexagonal structure (phase α) and body-centered cubic (phase β). The existence of aluminum and vanadium causes the α and β phases to stabilize, respectively, maintaining the dual phase at room temperature [22]. In general, the microstructure, when depositing material, presents a martensitic phase (α′) due to the rapid cooling

of the manufacturing process. In addition to the quick cooling, the α′ phase will only form if the build temperature is kept below the martensite start temperature (Ms) [30]. The aforementioned temperature varies from 575 °C up to 800 °C [31–33] as the impure elements along with the initial microstructure and composition homogeneity affect the Ms temperature [34]. In Figure 2, it is possible to analyze how the phase transformation is affected by the distinct cooling rates, i.e., in the region of 525–410 °C/s the α′ phase will be formed; however, if the cooling rate is kept under 20 °C/s, it will lead to the formation of the phase α.

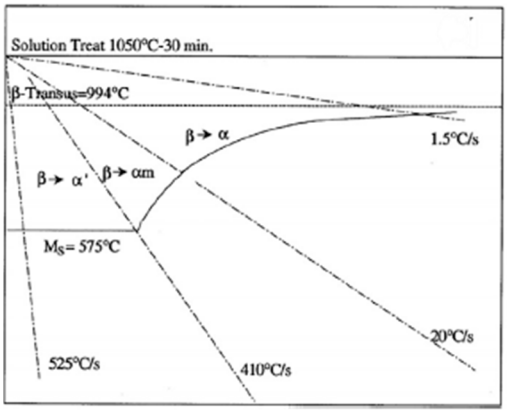

Figure 2. Diagram that explains how the cooling rate affects the phase transformation. Reproduced from [35], under CC BY 4.0.

In laser-based additive manufacturing processes, RS are induced by thermal principles, as the gradient temperature is high because of the heating and thermal expansion upon the deposition of a new layer, and its subsequent cooling and contraction [36]. Therefore, production errors in the components might occur due to geometrical distortion. Thus, it is mandatory to understand the expected orientation and magnitude of the RS in order to do accurate predictions of the final part properties. Moreover, high magnitude (100–500 MPa) RS are more prone to occur in the SLM rather than in the EBM process [37].

As a matter of fact, residual stresses can be divided into three different types, Type I, II, and III, depending on the operational length scale, as shown in Figure 3. Type I are macroscopic stresses that act on the scale of component geometry, Type II, often called intergranular stresses, are microstresses acting at the individual grain scale, and Type III act at the atomic scale [38]. Nowadays, multiple techniques are employed to measure residual stresses, and they can be divided into two major groups: destructive, and non-destructive testing. On one hand, if one seeks to find residual stresses located on the surface level in a non-destructive way, X-ray Diffraction (XRD) is one of the most suitable techniques for that effect due to its great accuracy (±20 MPa) and the large variety of equipment available [39]. On the other hand, if the goal is to investigate internal residual stresses in a destructive way, one can use the stripping method, crack compliance method, or the contour method. Furthermore, there is also an economic semi-destructive way to discover surface residual stresses called the hole-drilling strain gage method [40]. It is considered a semi-destructive method as it does not affect, in a significant way, the structural integrity of the part. Currently, an ISO standard does not exist; however, according to American Society for Testing and Materials (ASTM) E837-08 [41] standard, the aforementioned method can be described as a technique that computes residual stresses near the surface of a material by sticking a strain rosette to the part's surface and then drilling a hole at the center of the rosette, which later determines the relieved strains.

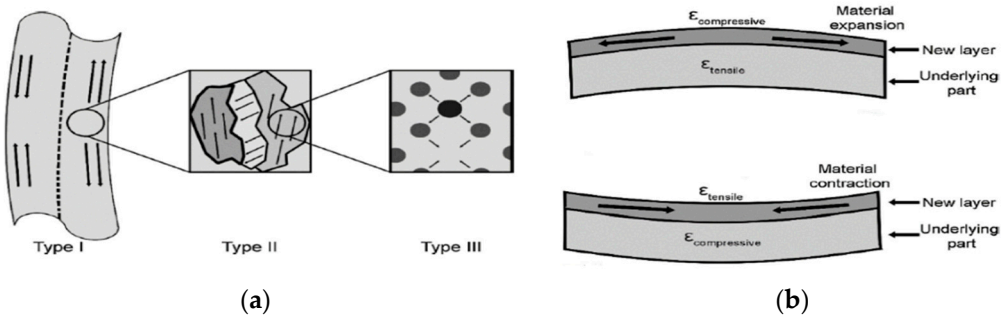

Figure 3. (**a**) Residual stresses classification and (**b**) plastic deformation development. Reproduced from [36], with permission of Elsevier, 1996.

The research novelty of this work is the aggregation of all kinds of information from the last 20 years of research about the Ti–6Al–4V alloy in a structured way, namely information related to residual stresses, as well as the influence played by different heat treatments in reducing porosity, increasing mechanical properties, and the stress relief of additive manufactured components. The authors strongly believe that the compilation of the aforementioned data is essential because it allows understanding the research evolution of this titanium alloy, and it provides a good starting point for those who want to learn about additive manufacturing. Furthermore, the reading of this review paper can also be useful to understand some key aspects of the Ti–6Al–4V alloy, thus improving the quality and performance of the manufactured parts.

2. Methodology

The methodology followed in this article started with the selection of the theme, which is heat treatments and residual stresses on metal powder bed fusion Ti–6Al–4V parts. In this way, the authors tried to analyze the amount of information available on the ScienceDirect platform in order to get a general idea of the number of articles published on this topic. When performing an advanced search by title, abstract, and keywords on the topics "Additive Manufacturing + Ti-6Al-4V", 537 articles were found, of which only 11 were review articles, as shown in Figure 4.

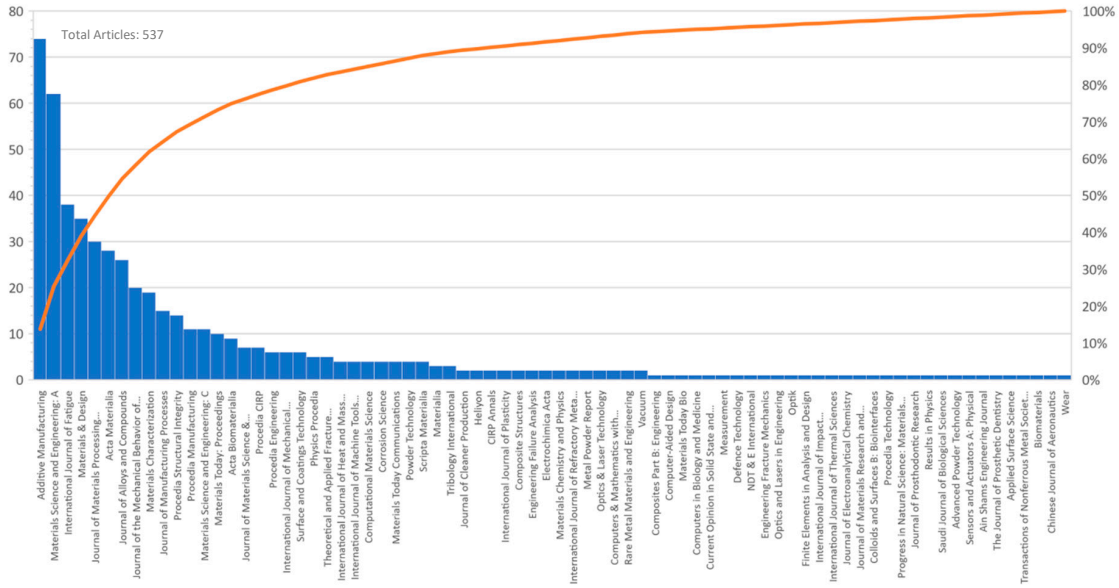

Figure 4. Pareto's chart of the research "Additive Manufacturing + Ti–6Al–4V" on ScienceDirect.

Then, after a thorough research for the topics "Heat Treatments + Selective Laser Melting + Ti-6Al-4V", as shown in Figure 5a, it was concluded that the number of results had decreased

considerably, with a total of 61 research articles. After that, the authors searched for "Residual Stresses + Selective Laser Melting + Ti–6Al–4V", as shown in Figure 5b, and they found that there were only 31 research articles. Lastly, the authors removed the word "Selective Laser Melting" on the last two searches and added the word "Electron Beam Melting", and they found out 18 articles about heat treatments and 10 about residual stresses, as shown in Figure 6. Note that if the research had not been done in an advanced way, the results would have been much higher; however, more than 50% of the results would not be relevant for this review article.

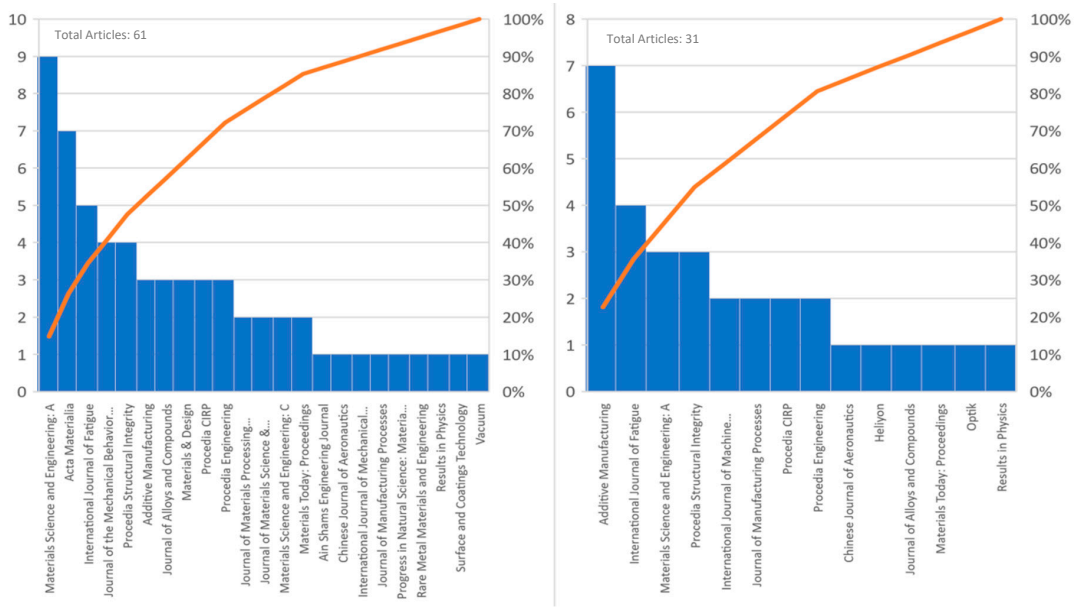

(**a**) (**b**)

Figure 5. Pareto's charts of the research, (**a**) "Heat Treatments + Selective Laser Melting + Ti–6Al–4V", and (**b**) "Residual Stresses + Selective Laser Melting + Ti–6Al–4V", on ScienceDirect.

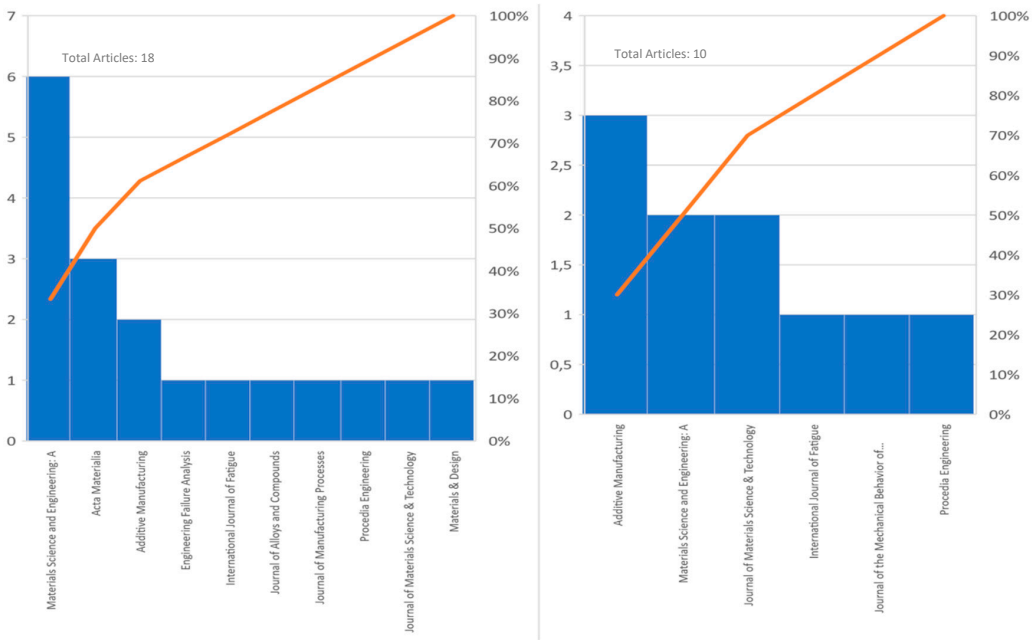

(**a**) (**b**)

Figure 6. Pareto's charts of the research, (**a**) "Heat Treatments + Electron Beam Melting + Ti–6Al–4V", and (**b**) "Residual Stresses + Electron Beam Melting + Ti–6Al–4V", on ScienceDirect.

3. Literature Review

Before heading to the first subsection of the literature review, the authors thought that the SLMed and EMBed as-built microstructures of the titanium alloy should be compared as they are heavily dependent on the manufacturing process. Furthermore, the microstructure also plays a crucial role in governing the material properties of the components. Therefore, several investigators studied the as-built microstructure of SLMed titanium samples [42–46]. Thijs et al. [42] reported that all the as-built specimens produced via SLM showed a microstructure with fine acicular α′ precipitates in the columnar original β grains, which was due to the rapid cooling of the manufacturing process, as shown in Figure 7a. Similarly, Facchini et al. [43] and Gong et al. [44] found the same microstructure results as the aforementioned study, while Benedetti et al. [45] reported that the as-built titanium specimens had a very fine acicular α′ microstructure. On the contrary, Xu et al. [46] managed to accomplish an ultrafine lamellar α + β structure of SLMed titanium as-built specimens without having notable grain coarsening. The authors used the following process variables: layer thickness of 60 µm, focal offset distance of 2 mm, and energy density of 50.62 J/mm^3, they and reported that a careful selection of the printing parameters was the key for such microstructure.

Several other authors studied the microstructure of as-built titanium specimens produced via EBM [47–51]. Xu et al. [47] reported that an α + β lamellar microstructure, as shown in Figure 7b, was achieved for the following processing parameters: accelerated voltage of 60 kV, beam current of 10 mA, filament current of 432 mA, focus current of 670 mA, gun vacuum pressure of 3.4×10^{-3} Pa, chamber vacuum pressure of 7×10^{-2} Pa, and work distance of 150 mm. Likewise, Galarraga et al. [48], Zhao et al. [49], Chern et al. [50], and Murr et al. [51] found an α + β lamellar microstructure in the EBMed as-built specimens.

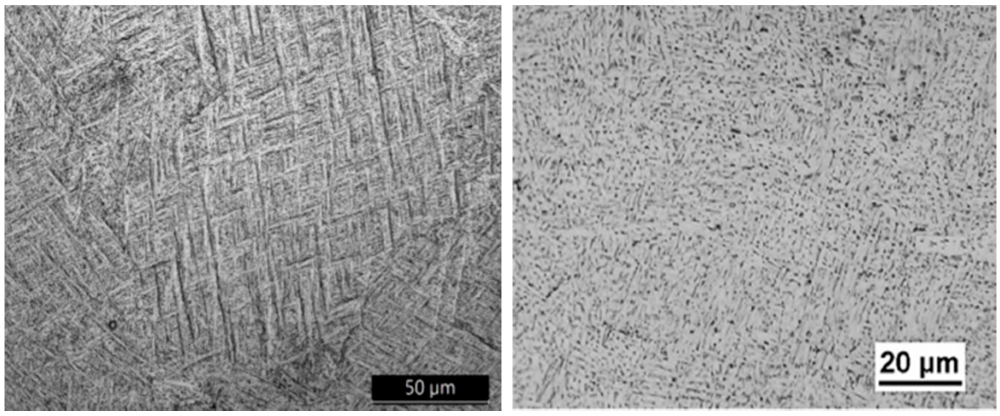

(**a**) (**b**)

Figure 7. Characteristic microstructure of (**a**) SLM process (fine acicular α′ in columnar original β grains), and (**b**) EBM process (α + β lamellar). Reproduced from [45,48] respectively, with permission of Elsevier 2017, 2016.

Furthermore, it is also relevant to understand the influence played by distinct additive manufacturing processes on the mechanical properties, profile surface roughness (Ra), and porosity of Ti–6Al–4V components. Thus, in Table 1, it is possible to analyze the distinct as-built mechanical properties of titanium samples. From the aforementioned table, it is worth noting that the SLMed samples, when compared to the EBMed ones, exhibit a 20% to 30% increase of the yield strength (YS) and ultimate tensile strength (UTS); however, the ductility is much lower due to the inherent rapid cooling of the SLM process which promotes an α′ martensitic microstructure within long columnar prior β grains. Regarding the Ra, it is known that different scan speeds, powder sizes, and layer thicknesses of the EBM and SLM manufacturing processes promote distinct surface roughness [35]. Edwards et al. [52] stated that the titanium specimens produced via SLM had an Ra between 32 and 38.5 µm, depending on the build orientation. Moreover, Chan et al. [53] compared the surface roughness

of Ti–6Al–4V samples manufactured via SLM and EBM and reported that the latter manufacturing process revealed an Ra of 131 µm, while the former presented 38.5 µm. The authors associated the high surface roughness of the EBMed sample to the presence of unfilled gaps and unmelted powder attached to the surface. Fousová et al. [54] studied the effect of internal defects and surface roughness on the mechanical properties of Ti–6Al–4V samples produced via SLM and EBM. In order to achieve a similar microstructure as the EBM as-built specimens, the SLM ones underwent a heat treatment at 820 °C for 5.5 h. After analyzing the microstructure and conducting a uniaxial tension test and a fatigue test, the authors reported that both EBMed and SLMed specimens exhibited a two-phase lamellar microstructure; however, internal defects were distinct due the manufacturing process. EBMed samples showed spherical pores resulting from gas entrapment, while SLMed ones revealed insufficient melting defects. Despite that, the researchers concluded that the static properties in the tension of both samples reached comparable values, but the fatigue test demonstrated that the SLMed specimens exhibited greater fatigue strength (220 ± 24 MPa) than the EBMed ones (115 ± 13 MPa) due to the lower surface roughness. Besides, Qiu et al. [55] studied the effect of laser power and layer thickness on surface roughness and porosity level of SLMed titanium as-built samples. The researchers reported that a low layer thickness combined with a high laser power leads to the production of specimens with a porosity level inferior to 1 vol%. In fact, when it comes to part porosity, several authors [44,49,56] reported that in the SLM process, one should expect porosities between 0.1 and 0.5 vol%, while others [44,57] stated that components produced through EBM present an inherent porosity between 0.1 and 0.3 vol%. Recently, Ning et al. [58] created an analytical model based on the relationship between porosity evolution and the thermal behavior of the material, which predicted part porosity in metal powder bed additive manufacturing without resorting to any iteration-based simulations or Finite Element Modeling (FEM). For that, the authors followed the algorithm that can be seen in Figure 8. The molten pool dimensions were computed through the comparison of the material's melting temperature with the expected temperatures using an analytical thermal model. The porosity evaluation was computed by subtracting the volume fraction of the powder bed void from the post-processed porosity of the part. The volume fraction of the powder was investigated by image analysis and through an advancing front approach. Then, after determining the analytical results of the expected porosity, the authors compared the values with additively manufactured Ti–6Al–4V specimens from the literature and concluded that their model could predict porosity with a high amount of precision. Furthermore, the authors stated that the computational time of the model was short, allowing a quick and precise prediction for distinct processing parameters.

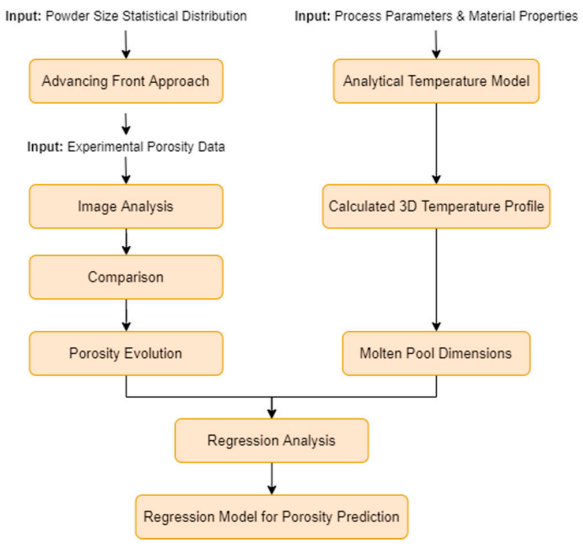

Figure 8. Schematic illustration of the algorithm used in the porosity prediction model. Adapted from [58], with permission of Elsevier, 2020.

In another report, Zhang et al. [59] studied and compared the wear resistance of as-built SLM, as-built EBM, and forged Ti–6Al–4V samples. Then, the authors performed friction and wear tests to the three types of samples and concluded that when compared to the forged specimens, the additively manufactured ones exhibited a better wear resistance owing to their weaker delamination and higher hardness. Moreover, the SLMed samples showed a higher wear rate than the EBMed ones due to the higher number of horizontal cracks of the former, as shown in Figure 9.

Table 1. Mechanical properties of as-built Ti–6Al–4V specimens in tensile testing. UTS: ultimate tensile strength, YS: yield strength.

Manufacturing Process	YS [MPa]	UTS [MPa]	ε [%]	Ref.
EBM	881 ± 12.5	978.5 ± 11.5	10.7 ± 1.5	[60]
EBM	851.8 ± 5.8	964.5 ± 0.3	16.3 ± 0.8	[61]
SLM	1056 ± 29	1351 ± 34	5.5 ± 0.8	[62]
SLM	1143 ± 30	1219 ± 20	4.9 ± 0.6	[63]

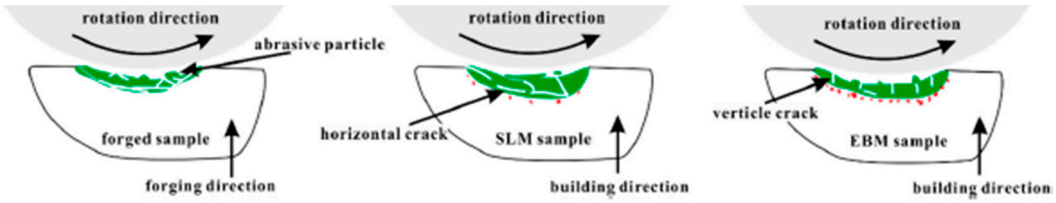

(**a**) (**b**) (**c**)

Figure 9. Wear mechanisms in the Ti–6Al–4V samples built by (**a**) forging, (**b**) SLM, and (**c**) EBM. Reproduced from [59], under CC BY 4.0.

3.1. Heat Treatments

Heat treatments are known for reducing residual stresses, improving mechanical properties, and changing the microstructure of titanium components. Balyakin et al. [64] studied the heat treatment effect on the surface roughness of titanium specimens manufactured via SLM. The researchers conducted distinct heat treatments followed by mechanical brushing and chemical polishing and reported that after heating the samples to 950 °C for 30 min followed by oil quenching and subsequent aging at 650 °C for 120 min, the specimens exhibited the worst surface roughness (Ra = 4.41 μm) measured just before undergoing mechanical polishing and chemical polishing, whilst the best final surface roughness (Ra = 0.27 μm) was achieved through the following preliminary heat treatments: annealing at 650 °C for 120 min followed by furnace cooling (FC) plus heating up to 950 °C for 30 min followed by water quenching (WQ). Vayssette et al. [65] investigated the roughness influence on multiaxial high-cycle fatigue of titanium samples manufactured via SLM and EBM. Firstly, when producing the specimens, the authors used processing parameters that minimized the RS formation due to high-thermal gradients. Secondly, the samples were post-treated with a stress relief heat treatment followed by Hot Isostatic Pressing (HIP), which aimed to reduce each part's porosity. After that, the researchers analyzed the microstructure and reported that both samples exhibited a lamellar microstructure with a mean 2 μm lamella size. Then, the authors measured the Ra values of both samples before and after chemical polishing, which for the SLM samples were 18.9 μm and 11.2 μm, and for the EBM, they were 38.9 μm and 17.7 μm, respectively. Finally, the researchers conducted fatigue tests and reported that despite the roughness improvement induced by the chemical etching, the fatigue properties did not improve significantly. Similarly, Yuan et al. [66] investigated the heat treatment effect on the compressive fatigue properties of titanium samples produced via EBM. For that, after manufacturing the samples, the authors conducted an annealing treatment with three different temperatures (750 °C, 850 °C, and 950 °C) for 1.5 h followed by FC to room temperature. Then, they compared the as-built microstructure to the post-treated one and concluded that the heat treatment promoted the decomposition of the acicular α' martensite into

an α + β phase. After conducting fatigue tests, the researchers concluded that when annealing at 950 °C, near the phase boundary, the width of the α lamellae coarsens up to 20 μm and promotes a ductility improvement of the struts, an increase of the fatigue strength, and the fatigue endurance ratio raises to nearly 0.6, which is almost three times more than that reported in another work [67].

Several authors [68–73] studied the fatigue properties of the titanium alloy manufactured via metal powder bed fusion. Chastand et al. [68] investigated the influence of different manufacturing processes, build orientation, surface roughness, and HIP treatment on the fatigue life of titanium samples. To do that, the researchers manufactured several specimens in SLM and EBM machines with different build orientations, namely XY and Z. Then, all the SLMed specimens underwent a stress relief treatment at 640 °C for 4 h, while others undertook a stress relief + HIP treatment at 920 °C under 1020 bar for 2 h. After that, the authors conducted the same HIP treatment to 12 EBMed specimens and then machined and polished the surface of several SLMed and EBMed samples. After conducting the fatigue tests, Chastand et al. [68] reported that the manufacturing processes (SLM and EBM) effect is negligible on the fatigue properties, as a similar type of defects was found in both cases. Moreover, machining and polishing improved the fatigue properties of the titanium alloy because it lowered the surface roughness and removed superficial defects. Furthermore, the HIP treatment led to the size decrease of the internal defects, hence improving the fatigue properties. To conclude, the authors also reported that the effect of the build direction highly depends on the presence of unmelted zones. In a similar study, Wu et al. [71] investigated the porosity and HIP treatment effect on the fatigue endurance ratio of SLMed titanium samples. For that, the researchers purposely manufactured cellular structures with three different porosities (33 vol%, 50 vol%, and 84 vol%) and then subjected some of them to an HIP treatment at 1000 °C and a pressure of 150 MPa for 1 h. After studying the microstructure, the authors reported that the heat treatment promoted the transformation of the martensitic microstructure into a lamellar α + β phase. Then, the researchers conducted fatigue tests and concluded that the porosity increase in the as-built samples led to a decrease in the fatigue endurance ratio, as shown in Figure 10, due to the low ductility of α′. However, in the HIPed samples, as the porosity increased from 33 vol% to 50 vol%, the fatigue endurance ratio at 10^6 cycles increased from 0.5 up to nearly 0.55, Figure 10. Moreover, when compared to the as-built specimens, the HIPed ones exhibited far better fatigue endurance ratios as the porosity increased. Similarly, Vispoli et al. [72] investigated the surface roughness effect on the fatigue behaviour of Ti–6Al–4V samples produced via SLM. The authors reported that the fatigue resistance of the as-built specimens, when compared to the machined ones, evidenced a drastic reduction due to the elevated roughness.

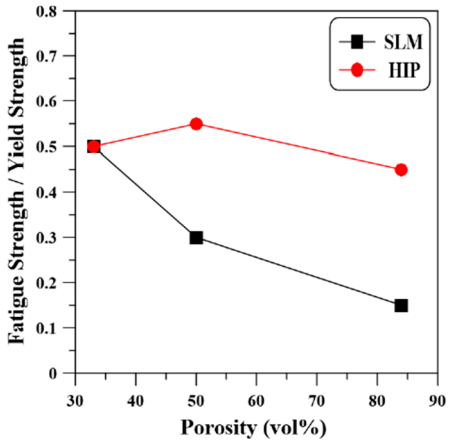

Figure 10. Porosity influence on the fatigue endurance ratios at 10^6 cycles of as-built and specimens subject to Hot Isostatic Pressing (HIP). Reproduced from [71], with permission of Elsevier, 2020.

Likewise, Yu et al. [73] studied the influence of distinct heat treatments and surface finishing processes on the fatigue performance of titanium samples produced via SLM. The authors employed

four different finishing processes, namely turning, 400 mesh sandpaper grinding, 400 mesh sandpaper grinding + sandblasting, and polishing. Furthermore, the researchers also conducted three distinct heat treatments, which can be seen in Table 2. After the fatigue tests, the authors concluded that all the surface-finishing processes reduced the as-built arithmetic mean roughness (Ra = 12.16 μm), hence significantly improving the fatigue performance of the samples. Furthermore, as is possible to analyze in Figure 11a, when compared to the as-built specimens, the HIPed and HT-920 ones showed lower YS and UTS; however, the ductility was greatly improved. On the contrary, the HT-850-550 specimens showed no obvious reduction in the YS and UTS when compared to the as-built ones, and the ductility of the former specimens was also better than the latter. Finally, the heat treatments promoted the increase of the fatigue limit, as the HT-920 and HT-850-550 samples exhibited a stress amplitude of approximtaely 400 MPa for 10^6 cycles, and the HIPed samples showed a stress amplitude of approximtaely 500 MPa for the same number of cycles, as shown in Figure 11b.

Table 2. Distinct heat treatments performed by Yu et al. [73]. FC: furnace cooling, WQ: water quenching.

Code Name in Figure 11a	Condition
SLMed	As-built
HIPed	HIP at 920 °C and a pressure of 100 MPa for 2 h
HT-920	Heat treatment at 920 °C for 2 h followed by FC
HT-850-550	Double heat treatment, firstly done at 850 °C for 2 h followed by WQ and then 550 °C for 4 h followed by AC

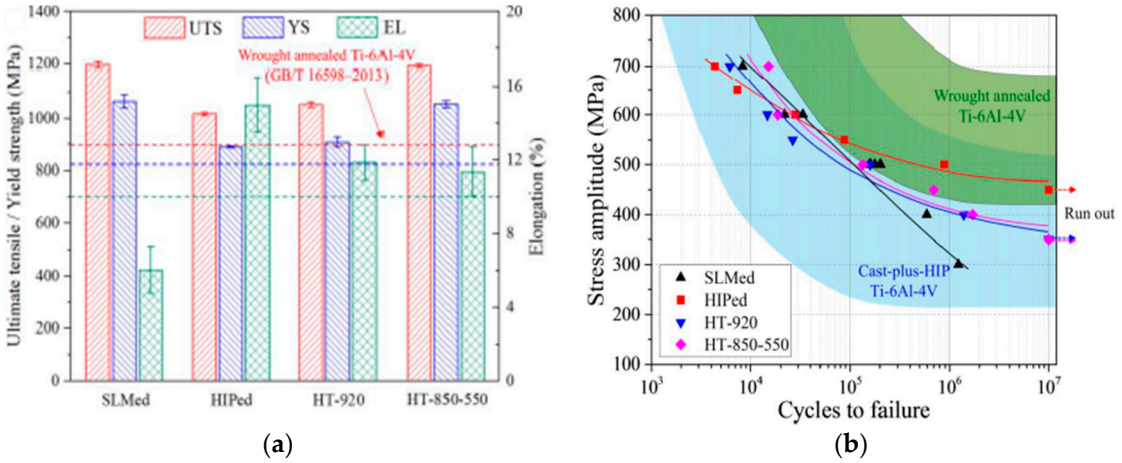

(**a**) (**b**)

Figure 11. (**a**) Tensile properties and elongation of the different specimens, (**b**) Fatigue performances of the distinct specimens. Adapted from [73], with permission of Elsevier, 2019.

Kim et al. [74] investigated the effect of microstructure control through heat treatments on the high-temperature creep behavior of Ti–6Al–4V specimens manufactured via SLM. The authors conducted a heat treatment at 1040 °C for 1 h and then analyzed the microstructure of the as-built and heat-treated specimens. The former exhibit a typical martensitic microstructure, while the latter showed a β phase at the interface of a large α colony area, meaning that a Widmanstätten's structure was formed. Subsequently, the researchers did two different mechanical tests, namely a compressive test at 500 °C and a high-temperature creep test, and they reported that the compressive yield strength of the as-built specimens was approximately 930 MPa and that in the heat-treated specimens was 557 MPa. Nevertheless, the high-temperature creep test results confirmed that the heat-treated samples exhibited a lower steady-state creep rate, proving that the martensitic microstructure has a lower creep performance than the Widmanstätten one.

In a different study, Ettefagh et al. [75] investigated the influence of the annealing heat treatment on the corrosion resistance of SLMed titanium components. For that, the authors conducted two distinct post-treatments at 600 °C and 800 °C for 2 h. The microstructure analysis revealed that the

heat treatment done at 600 °C did not provide the proper condition for the vanadium diffusion, hence the microstructure remained similar to the as-built one (α′ needle-like). However, the 800 °C heat treatment led to the formation of the β phase and the stress relief of the α′ phase. Then, the researchers performed the corrosion tests and ascertained that the corrosion rate of the as-built specimens was nearly 16 times worse than the cold-rolled commercial titanium samples, which were used as a benchmark. Moreover, the martensitic phase stress relief and the formation of the β phase on the 800 °C post-treated samples greatly improved the corrosion behavior of the material, which exhibited results comparable to the benchmark.

Wang et al. [76] studied the heat treatment effect on the biocompatibility and osseointegration of SLMed titanium samples. For that, the researchers employed an annealing treatment at a temperature of 820 °C for 4 h to half of the manufactured specimens. Then, all the specimens were ultrasonic degreased in acetone and anhydrous ethanol baths for 1 h, respectively. Later, the authors applied human bone mesenchymal stem cells (hBMSCs) to both types of specimens, measured cell proliferation on the first, fourth, and seventh day of incubation, and reported that the heat-treated specimens showed a significant enhancement of hBMSCs adhesion and proliferation. The authors concluded that the annealing treatment promoted better mechanical properties, a more homogeneous, rougher, and more hydrophilic surface, as well as the formation of a crystalline rutile (TiO2) layer, which elevated the corrosion resistance and biocompatibility of the implant. Similarly, Pazhanivel et al. [77] investigated the post-treatment effect on the corrosion resistance of titanium specimens produced via SLM. Firstly, the authors produced several specimens on an EOS M290 machine using different laser power and scan speed parameters. After performing a tensile test, the researchers reported that the specimen that achieved the best elongation (10.88%) was manufactured with a laser power of 310 W and a scan speed of 1340 mm/s. Then, the researchers subjected some specimens to a heat treatment at 850 °C for 2 h and continued for 2 h more to go through isothermal heating. After that, the furnace temperature was set below 200 °C to reduce the specimen's temperature to 200 °C within 1 h, and, besides, the samples were also shot-peened. Later, the authors studied the microstructure of the as-built and post-treated Ti–6Al–4V samples and reported that the former exhibited the α′ as a major phase, while the latter was composed of ultrafine grain lamellar α + β phases. Subsequently, corrosive tests were performed in a NaCl and phosphate buffer corrosion media, and the researchers concluded that due to the microstructural change, the post-treated samples demonstrated lower corrosion rates. Likewise, Leon et al. [78] investigated the HIP effect on the corrosion performance of Ti–6Al–4V samples manufactured by EBM. After producing the specimens, the authors conducted a thermal treatment at 925 °C with a pressure of 100 MPa for 3 h and then performed electrochemical measurements and stress-corrosion examination by means of slow strain-rate testing. After analyzing the results, the authors concluded that the heat treatment had a slightly advantageous effect on the mechanochemical performance and corrosion resistance of the titanium alloy due to the reduction of α/β interphase area, the increased amount of β phase, as well as the amplified passivation film stability.

Despite not using any thermal treatment, Sharma et al. [79] investigated the corrosion resistance of as-built Ti–6Al–4V bioimplants manufactured through SLM, having in mind that their dissolution inside the human body usually leads to inflammations in the internal organs. The authors used three types of corrosion media (NaOH, NaCl, and H2SO4), which varied from alkaline to acidic and also used a physiological simulated body fluid (SBF) medium as a comparison. Then, after manufacturing the samples, the researchers studied the microstructure of the SLMed and commercial cast titanium, which was used as a reference, and determined that the former exhibited a martensitic microstructure, while the latter showed a uniform distribution of α + β phases. Subsequently, the authors conducted several corrosion tests and reported that the SLMed samples had a worse corrosion resistance than the reference because of the α′ phase and the higher surface porosity. Nevertheless, the charge transfer resistance, which measures the difficulty faced when an electron is moved from one atom/compound to another, and the polarization of both samples were noticeably high in NaOH, NaCl, and SBF, meaning

that the samples exhibited a good corrosion resistance in the aforementioned media. However, in a more acidic and aggressive solution (H2SO4), they showed an enormously poor corrosion resistance.

Nalli et al. [80] investigated the barrel finishing and heat treatment effect on the mechanical properties of Ti–6Al–4V samples manufactured through SLM. For that, some specimens were heat-treated with distinct temperatures (482 °C, 704 °C, 788 °C, and 800 °C) and holding times (3 h, 4 h, 5 h, 6 h, 8 h, and 10 h). Furthermore, others were barrel finished at 30 and 42 rpm, and as a reference, the authors left some specimens in the as-built state. Then, mechanical tests were performed, and after analyzing the results, the researchers reported that as the temperature of the heat treatment and the intensity of the barrel finishing increased, the elongation at break of the specimens improved as well. However, as the elongation increased, the YS and UTS decreased; nevertheless, the authors concluded that the heat treatment temperature of 788 °C and barrel finishing speed of 30 rpm provided the best results in terms of ductility versus strength.

In order to have a better understanding of the effects caused by distinct post-treatments on the mechanical properties of Ti–6Al–4V components, the authors of the current work agglomerated distinct information from diverse scientific reports related to YS, UTS, and elongation at break (ε), which can be analyzed in Table 3.

Table 3. Manufacturing process and post-treatment effect on the mechanical properties of the Ti–6Al–4V alloy.

Mnf. Process	Condition	Orientation	YS [MPa]	UTS [MPa]	ε [%]	Ref.
Wrought	-	Vertical	836 ± 9	942 ± 8	12.5 ± 1.2	[81]
Wrought	-	Horizontal	832 ± 10	933 ± 7	13.0 ± 1.5	[81]
Forged	Mill Annealed	-	970	1030	16	[82]
Forged	Mill Annealed	-	960 ± 10	1006 ± 10	18.37 ± 0.88	[83]
Cast	-	-	865	980	13.5	[84]
Cast	-	-	750 ± 2	875 ± 10	4.5 ± 0.2	[85]
ASTM F136	-	-	≥795	≥860	≥10	[86]
EBM	As-built	Vertical	812 ± 12	851 ± 19	3.6 ± 0.9	[87]
EBM	As-built	Horizontal	783 ± 15	833 ± 22	2.7 ± 0.4	[87]
EBM	As-built	Vertical	869 ± 7.2	928 ± 9.8	9.9 ± 1.7	[63]
EBM	As-built	Horizontal	899 ± 4.7	978 ± 3.2	9.5 ± 1.2	[63]
EBM	As-built	Vertical	1001–1051	1073–1116	11–15	[82]
EBM	As-built	Horizontal	973–1006	1032–1066	12–15	[82]
EBM	HIPed	-	723–817	817–918	3–9	[88]
EBM	Two-stage HIPed	-	885 ± 6	985 ± 12	-	[89]
EBM	Annealed	-	741–842	837–918	3–9	[88]
EBM	Stress Relieved	-	778–943	885–1015	3–9	[88]
SLM	As-built	Vertical	1150 ± 67	1246 ± 134	1.4 ± 0.5	[81]
SLM	As-built	Horizontal	1273 ± 53	1421 ± 120	3.2 ± 0.5	[81]
SLM	As-built	Vertical	1143 ± 30	1219 ± 20	4.89 ± 0.6	[63]
SLM	As-built	Horizontal	1195 ± 19	1269 ± 9	5.0 ± 0.5	[63]
SLM	HIPed	Vertical	883–888	973 – 974	18.5–19.4	[90]
SLM	HIPed	-	912 ± 30	1005 ± 30	8.3 ± 2	[91]
SLM	Annealed	Vertical	1045–1054	1115–1116	9.5–12.4	[90]
SLM	Annealed	Vertical	905–911	987–989	7.4–12.5	[90]
SLM	Annealed	Horizontal	913 ± 7	1019 ± 11	8.9 ± 1	[84]
SLM	Annealed	Horizontal	944 ± 8	1036 ± 30	8.5 ± 1	[84]
SLM	Stress Relieved	Vertical	937 ± 9	1052 ± 11	9.6 ± 0.9	[92]

Similarly, several authors [92–100] also studied the heat treatment effect on the mechanical properties and microstructure of Ti–6Al–4V components. For instance, Benzing et al. [92] demonstrated the efficiency of a novel HIP treatment strategy employed to EBMed specimens. The heat treatment consisted of a two-stage HIP, which can be described as follows: 1050 °C with a pressure of 100 MPa for 2 h with a 12 °C/min heating rate and a nearly 1600 °C/min cooling rate done between 1050 and 500 °C + temper HIP at 800 °C with a pressure of 30 MPa for 2 h and 12 °C/min heating and cooling rates. After studying the microstructure and performing mechanical tests, the authors reported that the new heat treatment maintained the α lath thickness of 1.20 μm ± 0.32 μm, created prior-β grains,

sealed the internal porosity, removed microstructural heterogeneities, and maintained the YS and UTS identical to the as-built specimens. In another report, Sabban et al. [96] applied an innovative heat treatment strategy that achieves a bimodal globularized microstructure without the need for a previous plastic deformation process. After manufacturing the specimens in an SLM machine, the researchers employed a heat treatment, as shown in Figure 12, with a thermal cycle between 875 and 975 °C, a heating rate of 2.5 °C/min, and a cooling rate of 1 °C/min. The authors reported that the numerous heating cycles transformed the lamellar α phase into the β phase, which later transformed into globular α upon slow cooling. Moreover, the Electron Backscatter Diffraction (EBSD) micrograph showed that the heating cycles also aided to break the α lamella into smaller segments, which subsequently were converted into spatially separated globular α. Besides, the ductility of the heat-treated specimens, when compared to the as-built ones, was enhanced, the YS and UTS suffered a small decrease, the toughness increased from 98 to 163 MJ/m^3, and beneficial compressive residual stresses were created at the surface level. Likewise, Galarraga et al. [98] submitted EBMed titanium specimens to different solution heat treatments with distinct cooling rates and reported that the water-cooled samples, when compared to the furnace-cooled ones, exhibited an utterly α′ martensitic microstructure which promoted an increase of 31 % of the UTS; however, they lowered the ductility by 86%. Haar et al. [100] developed a novel duplex anneal treatment that was firstly done at 910 °C for 8 h followed by water-quenching and then 750 °C for 4 h followed by furnace-cooling. The first step of the heat treatment created a bimodal microstructure of α in the α′ matrix, while the second step promoted the decomposition of α′ into α + β lamellar. Subsequently, the authors conducted tensile tests and verified that when compared to the as-built SLMed and conventionally annealed samples, the duplex annealed ones demonstrated a far greater ductility.

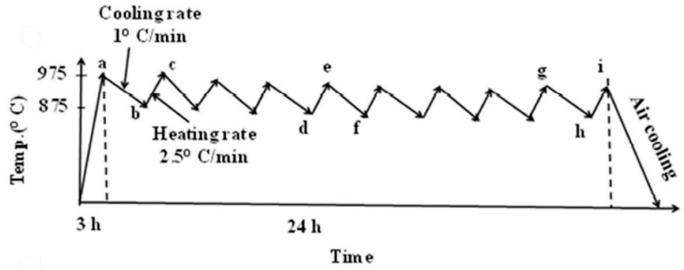

Figure 12. Schematic of the heat treatment employed for a period of 24 h. Reproduced from [96], with permission of Elsevier, 2019.

3.2. *Residual Stresses*

In additive manufacturing, residual stresses are spatially nonuniform and can lead to worse fatigue life and mechanical properties of the built components, as well as layer delamination and part distortion [101]. Moreover, the length of the scan vectors used when producing the components can also influence the distribution and magnitude of RS, as a longer scan vector results in a higher temperature gradient, which is opposite to shorter scan vectors that are preferable to create lower residual stresses [102]. Hence, one of the most usual scanning strategies employed is the chessboard scanning [103]. Ali et al. [104] investigated the effect of the scan strategy and vector length on SLMed Ti–6Al–4V specimens. For that, the authors used distinct scan strategies, namely 45° alternating, 90° alternating, 2 mm × 2 mm chessboard, 3 mm × 3 mm chessboard, 5 mm × 5 mm chessboard, 5 mm × 5 mm chessboard with scan vectors rotated 45° in adjacent blocks, and 5 mm × 5 mm chessboard with scan vectors rotated 90° in adjacent blocks. After analyzing the finite element simulation results, the researchers reported that a 90° alternating scan strategy caused the lowest residual stresses. Furthermore, the growth of the scan vector length in the chessboard scanning strategy resulted in increased residual stresses. Likewise, Song et al. [105] used finite element simulation and experimental verification to ascertain the effect of scanning strategies on the residual stresses of SLMed Ti–6Al–4V samples. The authors employed three distinct scan strategies, which were

line scan, 15° alternating scan, and 90° alternating scan. After conducting several tests, they reported that the scan strategy had little to no influence on the molten pool size, and the 15° alternating scan strategy produced the lowest residual stresses. Lu et al. [106] investigated the RS evolution on distinct chessboard scanning areas through Vickers micro-indentation. After performing the aforementioned test, the authors reported that the lowest RS were found in the 2×2 mm^2 sample; however, that only happened because cracks were formed, and stresses were released. Thus, the authors concluded that the 5×5 mm^2 scanning area was the best to produce end parts with the lowest RS.

Laser Shock Peening (LSP) has been widely studied by several authors [107–114], which state that the aforementioned post-treatment refines the microstructure and induces compressive residual stresses on the surface level, thus enhancing the fatigue lifetime of the components made from distinct titanium alloys. Zhang et al. [110] conducted a residual stress analysis through XRD and a micro-hardness test through Vickers indentation and reported that the LSP treatment induced compressive residual stresses and enhanced the micro-hardness of the Ti–6Al–4V samples. Plus, multiple laser shocks had a positive effect on the surface hardening. Furthermore, the authors also ascertained that the number of overlapped laser spots, which were meant to act as the laser peening intensity, provided better fatigue life properties when set to 3. In another study, Ren et al. [111] reported that the LSP treatment was able to reduce the surface roughness and repair surface details of Ti–6Al–4V samples if done with a lower laser pulse energy (6.3 J). Besides, when the authors employed a higher laser pulse energy (7.9 J), the surface hardness significantly increased. Likewise, Jin et al. [113] investigated the influence of LSP on the fatigue behavior and microstructure of Ti–6Al–4V samples manufactured via EBM. For the post-treatment, the authors used a Nd:YAG laser with a frequency of 1 Hz, a wavelength of 1064 nm, a beam diameter of 2.5 mm, and a pulse duration of 12 ns. Then, the microstructure was studied, and the researchers reported that the EBMed specimens showed a microstructure composed of $\alpha + \beta$ phases, as shown in Figure 13a. Besides, the LSP treatment caused grain refinement of the α phase via deformation twinning, as shown in Figure 13b. Subsequently, the authors performed mechanical tests and concluded that the LSPed samples, when compared to the as-built ones, exhibited a micro-hardness increase of 11%, as well as a run-out fatigue strength (2×10^6 cycles) increase of 100 MPa. Moreover, the LSP treatment inhibited the crack initiation and enhanced the required work of fatigue fracture, which, according to the literature reviewed by the authors, was due to the formation of compressive residual stresses and the grain refinement. In a similar study, Lan et al. [114] investigated the effect of the LSP treatment on the microstructural evolution and mechanical properties of Ti–6Al–4V specimens. The authors employed the same LSP parameters as Jin et al. [113] and then studied the microstructural evolution of the as-built and post-treated samples. They reported that when compared to the as-built samples, the post-treated ones exhibited a refined α lamella into sub-micro-equiaxed grains and nano-equiaxed grains. Later, the researchers measured the residual stresses of both types of samples through XRD and concluded that the LSP treatment changed the surface stress state from nearly 45 MPa to −380 MPa. Finally, the authors conducted a tensile test and ascertained that the LSP-treated samples possessed a higher tensile strength and elongation, due to the grain refinement and the induced compressive RS.

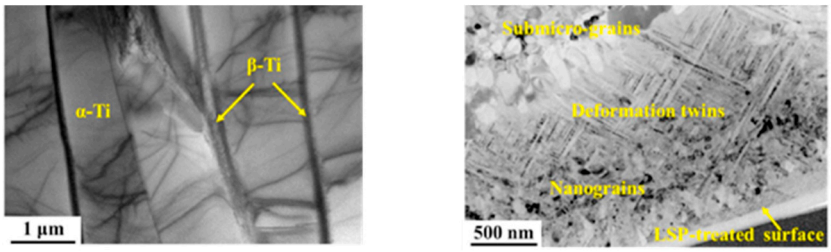

(**a**) (**b**)

Figure 13. Transmission Electron Microscopy (TEM) image of (**a**) EBM as-built specimens, and (**b**) Laser Shock Peening (LSP)-treated specimens. Adapted from [113], with permission of Elsevier, 2020.

Eyzat et al. [115] studied the effect of distinct post-treatments on the mechanical properties, residual stresses, and roughness of Ti–6Al–4V samples manufactured via SLM. For that, the researchers employed a stress relief heat treatment at 400 °C for 2 h to some specimens and the previous heat treatment + Surface Mechanical Attrition Treatment (SMAT) to the others. The latter post-treatment uses a high frequency (20 kHz) ultrasonic generator, which leads to the vibration and subsequent impact of spherical balls into the specimen's surface and promotes plastic deformation. After performing mechanical tests, investigating the specimen's surface roughness, and analyzing the residual stresses through the XRD method, the authors concluded that SMAT treatment changed the RS from tensile (approximately 100 MPa) to compressive (approximately −300 MPa) as it can be seen in Figure 14, reducing by 80% the high surface roughness, and boosting the mechanical properties (YS, UTS, and micro-hardness) by 10% to 15%. Yakout et al. [116] studied the correlation between residual stresses and process parameters of SLMed Ti–6Al–4V samples. For that, the authors used the Renishaw AM 400 machine and the titanium grade 23 powder from the same enterprise. Then, several specimens were manufactured using distinct laser power (P), scanning speed (v), and hatch spacing (h), while the layer thickness (t) was kept constant at 40 µm. Note that the aforementioned process parameters are all correlated in the Volumetric Energy Density (Ev) formula, which is:

$$E_v = \frac{P}{v \times h \times t} \quad (1)$$

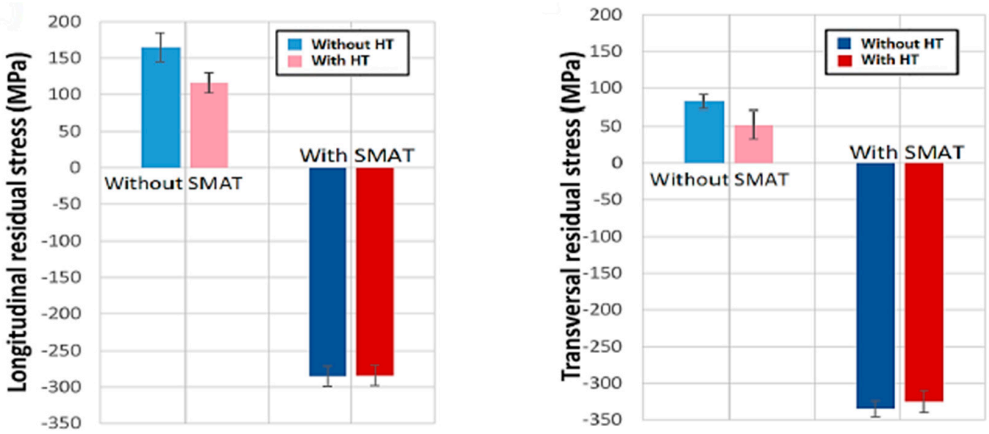

Figure 14. Post-treatment effects on (**a**) longitudinal residual stresses and (**b**) transversal residual stresses. Adapted from [115], under CC BY 4.0.

Later, after conducting distinct studies of the produced samples, the researchers concluded that the *Ev* increase led to a growth in the part's thermal expansion and density up to a maximum point, which was considered the critical energy density (*Ev* = 86.8 J/mm^3). Furthermore, the components manufactured with a volumetric energy density inferior to the critical one exhibited less residual stresses, as the XRD analysis exposed.

In a similar study, Vastola et al. [117] investigated, through FEM, the effect of beam scan speed, beam power density, beam size, and chamber bed temperature on the distribution and magnitude of residual stresses on EBMed Ti–6Al–4V samples. The authors reported that lower scan speeds deepened the Heat-Affected Zone (HAZ), while higher speeds reduce the HAZ. Furthermore, a 20% increase of the beam power caused an approximate 15% growth of the HAZ. Moreover, the researchers also stated that small beam sizes provided higher stresses within a smaller Heat-Affected Zone. Finally, it was concluded that the bed pre-heating temperature was the most crucial parameter for reducing the residual stresses, as a 50 °C increase of the pre-heating temperature promoted an approximate 20% decrease of residual stresses, as shown in Figure 15.

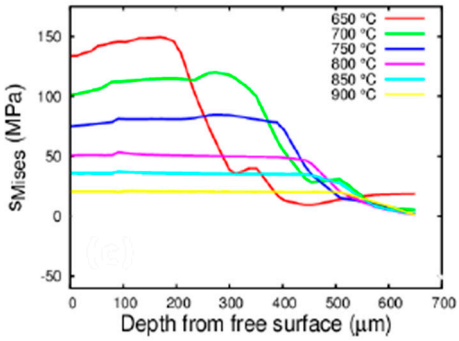

Figure 15. Quantitative effect of bed pre-heating temperature on residual stresses, where SMises is the Von Mises Stress. Adapted from [117], with permission of Elsevier, 2016.

In another study, Ning et al. [118] developed an analytical model that predicts RS and part distortion without the need for any iteration-based simulations or FEM. The inputs for the aforementioned model were the laser parameters, scan parameters, and material parameters, and the thermal model was calculated by a moving point heat source solution along with a heat sink solution. Then, the thermal stress model was calculated from the thermal model and the RS were computed from the thermal stress model by applying an elastoplastic relaxation method. After that, part distortion was computed using a surface displacement model, which finally outputted the distortion at distinct locations. The authors validated the accuracy of their analytical model by manufacturing several cantilever-like Ti–6Al–4V specimens on an SLM machine and measuring the part distortion on a Coordinate Measuring Machine (CMM). After comparing the experimental results with the analytical ones, the researchers ascertained that similar agreements were seen in terms of part distortion at distinct locations. Furthermore, the authors also emphasized that the computational time of the analytical model was only 10 s on a personal computer, thus allowing a high computational efficiency.

Finally, in Figures 16 and 17, it is possible to analyze two similar diagrams that explain and summarize the expected mechanical properties and microstructures of as-built and heat-treated EBMed and SLMed Ti–6Al–4V components, respectively.

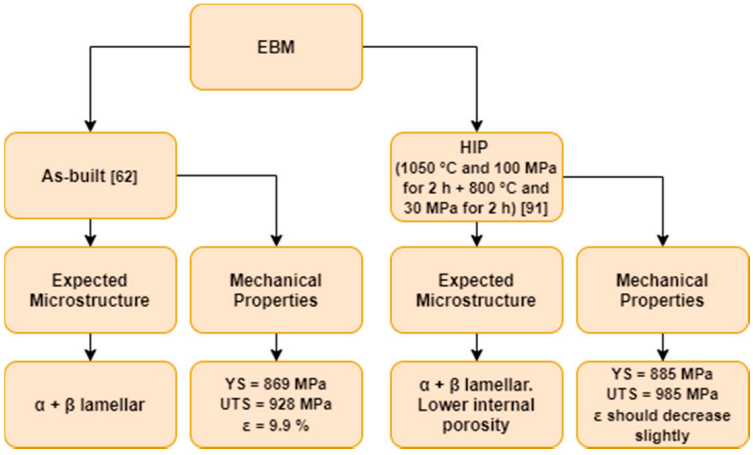

Figure 16. Diagram of the expected microstructure and mechanical properties of as-built and heat-treated EBMed Ti–6Al–4V samples.

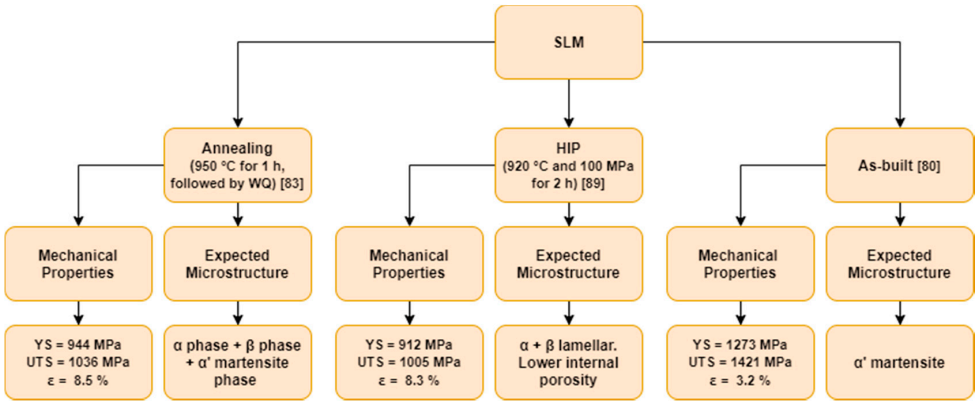

Figure 17. Diagram of the expected microstructure and mechanical properties of as-built and heat-treated SLMed Ti–6Al–4V samples.

4. Concluding Remarks and Outlook

One of the most used and studied superalloys in additive manufacturing is the Ti–6Al–4V, which can be applied in several distinct areas, namely in the aerospace field due to its low density and high melting point (around 1650 °C), and the biomedical area owing to its high corrosion resistance and excellent biocompatibility when in contact with tissues or bones of the human body. For this review work, the authors analyzed roughly 22% of the 537 different publications seen in Figure 4, and more than half of those 22% were about heat treatments and residual stresses of Ti–6Al–4V components produced via SLM and/or EBM in order to provide a solid and unbiased overview. The main ideas can be described as follows:

- Owing to the inherent characteristics of the SLM process, i.e., high cooling rates and quick solidification, the expected microstructure in the as-built state is characterized by fine acicular α′ martensitic precipitates in columnar original β grains, opposed to an α + β lamellar microstructure obtained through EBM. The latter manufacturing process achieves superior building chamber temperatures; therefore, it reduces the part's cooling rate and forms a bimodal microstructure.
- If one seeks to improve the mechanical properties, such as ductility and hardness, and decrease the residual stresses of SLMed Ti–6Al–4V parts, then heat treatments should be conducted. A duplex anneal treatment can be firstly done at 910 °C for 8 h followed by water-quenching and then 750 °C for 4 h followed by furnace-cooling. The first step of the heat treatment creates a bimodal microstructure of α in the α′ matrix, while the second step promotes the decomposition of α′ into α + β lamellar.
- Hot Isostatic Pressing must be done if one desires to increase the density and fatigue life of the manufactured component, as the aforementioned treatment is responsible for decreasing the size of the internal defects. Besides, one can also predict the expected porosity of the final pieces due to recent developments of trustworthy and efficient computer analytical models. Furthermore, the surface roughness also plays a crucial role in the fatigue life of the final part and is heavily dependent of the manufacturing process, i.e., SLM leads to lower Ra values than EBM; nevertheless, post-machining, sandblasting, and polishing can greatly decrease the Ra values, consequently weakening the crack initiation and improving the fatigue life.
- It has been seen that residual stresses can be lowered through heat treatments as well as optimized printing parameters, such as the bed pre-heating temperature in EBM or the correlation of distinct process parameters in the Volumetric Energy Density formula on SLMed components. Besides, high scanning speeds coupled with shorter scan vectors, i.e., chessboard scanning, has been demonstrated to lower the residual stresses. Furthermore, LSP and SMAT post-treatments can also enhance the fatigue life as they induce compressive residual stresses on the surface and increase the microhardness of the components.

Despite the tremendous research over the last years about additively manufactured Ti–6Al–4V parts, there are still some problems to overcome—namely, the mechanical properties variability when subjected to different heat treatments and process parameters. Furthermore, heat treatments should be further investigated and improved, because often one sacrifices yield and ultimate tensile strength for ductility. In addition, there is still room to improve regarding the residual stresses of Ti–6Al–4V components, i.e., researching the RS evolution under different heat treatments and printing parameters.

Lastly, the main limitations felt by the authors upon writing this review paper were the restricted access of several scientific articles as well as the comprehension of a small number of results exhibited by distinct authors. Moreover, as one can analyze in the Pareto charts (Figures 5 and 6), the scientific community has studied more SLMed Ti–6Al–4V components than EBMed ones, and only a few works focus on residual stresses, which ultimately was a big limitation of information.

Author Contributions: Conceptualization: Ó.T. and F.J.G.S.; methodology: Ó.T., L.P.F., E.A. and F.J.G.S.; investigation: Ó.T.; formal analysis: E.A., L.P.F. and F.J.G.S.; supervision: F.J.G.S. and E.A.; validation: F.J.G.S., L.P.F. and E.A.; writing original draft: Ó.T.; writing, reviewing and editing: F.J.G.S.; resources: E.A.; project administration: F.J.G.S., L.P.F. and E.A. All authors have read and agreed to the published version of the manuscript.

Funding: This research received no external funding.

Acknowledgments: The main author would like to acknowledge his mentor for all the help and support given through the writing of this report.

Conflicts of Interest: The authors declare no conflict of interest.

List of Symbols and Abbreviations

3DP	Three-Dimensional Printing
AM	Additive Manufacturing
ASTM	American Society for Testing and Materials
CMM	Coordinate Measuring Machine
EBM	Electron Beam Melting
EBSD	Electron Backscatter Diffraction
Ev	Volumetric Energy Density
FC	Furnace Cooling
FEM	Finite Element Modeling
h	Hatch Spacing
H2SO4	Sulfuric Acid
HAZ	Heat-Affected Zone
hBMSCs	Human Bone Mesenchymal Stem Cells
HIP	Hot Isostatic Pressing
ISO	International Organization for Standardization
LSP	Laser Shock Peening
Ms	Martensite Start Temperature
NaCl	Sodium Chloride
NaOH	Sodium Hydroxide
P	Laser Power
Ra	Surface Roughness
Ref.	Reference
RS	Residual Stresses
SBF	Simulated Body Fluid
SLM	Selective Laser Melting
SLS	Selective Laser Sintering
SMAT	Surface Mechanical Attrition Treatment
t	Layer Thickness
$T_{ambient}$	Ambient Temperature
T_{melt}	Melting Temperature

UTS	Ultimate Tensile Strength
v	Scanning Speed
WQ	Water Quenching
XRD	X-ray Diffraction
YS	Yield Strength
ε	Elongation at Break

References

1. Goldberg, D. History of 3D Printing: It's Older than You Are (That Is, If You're Under 30). AutoDesk. 2018. Available online: https://www.autodesk.com/redshift/history-of-3d-printing/ (accessed on 4 December 2019).
2. ISO/ASTM 52900-15. *Standard Terminology for Additive Manufacturing–General Principles–Terminology*; ASTM International: West Conshohocken, PA, USA, 2015.
3. Silva, F.J.G.; Campilho, R.D.S.G.; Gouveia, R.M.; Pinto, G.; Baptista, A. A Novel Approach to Optimize the Design of Parts for Additive Manufacturing. *Procedia Manuf.* **2018**, *17*, 53–61. [CrossRef]
4. Gouveia, R.M.; Silva, F.J.G.; Atzeni, E.; Sormaz, D.; Alves, J.L.; Pereira, A.B. Effect of Scan Strategies and Use of Support Structures on Surface Quality and Hardness of L-PBF AlSi10Mg Parts. *Materials* **2020**, *13*, 2248. [CrossRef]
5. ASTM F2792-12a. *Standard Terminology for Additive Manufacturing Technologies (Withdrawn 2015)*; ASTM International: West Conshohocken, PA, USA, 2012; pp. 1–3.
6. Meiners, W. Shaped Body Especially Prototype or Replacement Part Production. German Patent 19649865, 12 February 1998.
7. Giganto, S.; Zapico, P.; Castro-Sastre, M.Á.; Martínez-Pellitero, S.; Leo, P.; Perulli, P. Influence of the scanning strategy parameters upon the quality of the SLM parts. *Procedia Manuf.* **2019**, *41*, 698–705. [CrossRef]
8. Anwar, A.B.; Ibrahim, I.H.; Pham, Q.C. Spatter transport by inert gas flow in selective laser melting: A simulation study. *Powder Technol.* **2019**, *352*, 103–116. [CrossRef]
9. Ferrar, B.; Mullen, L.; Jones, E.; Stamp, R.; Sutcliffe, C.J. Gas flow effects on selective laser melting (SLM) manufacturing performance. *J. Mater. Process. Technol.* **2012**, *212*, 355–364. [CrossRef]
10. Konečná, R.; Nicoletto, G.; Riva, E. Notch fatigue behavior of Inconel 718 produced by selective laser melting. *Procedia Struct. Integr.* **2019**, *17*, 138–145. [CrossRef]
11. Contuzzi, N.; Campanelli, S.L.; Ludovico, A.D. 3D finite element analysis in the Selective Laser Melting process. *Int. J. Simul. Model.* **2011**, *10*, 113–121. [CrossRef]
12. Nguyen, Q.B.; Luu, D.N.; Nai, S.M.L.; Zhu, Z.; Chen, Z.; Wei, J. The role of powder layer thickness on the quality of SLM printed parts. *Arch. Civ. Mech. Eng.* **2018**, *18*, 948–955. [CrossRef]
13. Arcam, A.B. Arrangement for the Production of a Three-Dimensional Product. U.S. Patent 20060141089, 29 June 2006.
14. Körner, C.; Attar, E.; Heinl, P. Mesoscopic simulation of selective beam melting processes. *J. Mater. Process. Technol.* **2011**, *211*, 978–987. [CrossRef]
15. Galati, M.; Iuliano, L. A literature review of powder-based electron beam melting focusing on numerical simulations. *Addit. Manuf.* **2018**, *19*, 1–20. [CrossRef]
16. Li, P.; Warner, D.H.; Fatemi, A.; Phan, N. Critical assessment of the fatigue performance of additively manufactured Ti-6Al-4V and perspective for future research. *Int. J. Fatigue* **2016**, *85*, 130–143. [CrossRef]
17. Prabhakar, P.; Sames, W.J.; Dehoff, R.; Babu, S.S. Computational modeling of residual stress formation during the electron beam melting process for Inconel 718. *Addit. Manuf.* **2015**, *7*, 83–91. [CrossRef]
18. Smith, C.J.; Derguti, F.; Hernandez Nava, E.; Thomas, M.; Tammas-Williams, S.; Gulizia, S.; Fraser, D.; Todd, I. Dimensional accuracy of Electron Beam Melting (EBM) additive manufacture with regard to weight optimized truss structures. *J. Mater. Process. Technol.* **2016**, *229*, 128–138. [CrossRef]
19. Gokuldoss, P.K.; Kolla, S.; Eckert, J. Additive manufacturing processes: Selective laser melting, electron beam melting and binder jetting-selection guidelines. *Materials* **2017**, *10*, 672. [CrossRef]
20. Azam, F.I.; Abdul Rani, A.M.; Altaf, K.; Rao, T.V.V.L.N.; Zaharin, H.A. An In-Depth Review on Direct Additive Manufacturing of Metals. *IOP Conf. Ser. Mater. Sci. Eng.* **2018**, *328*, 012005. [CrossRef]
21. Properties of Titanium Ti-6Al-4V (Grade 5). Matweb. Available online: http://www.matweb.com/search/datasheet.aspx?MatGUID=10d463eb3d3d4ff48fc57e0ad1037434 (accessed on 6 December 2019).

22. Zuback, J.S.; DebRoy, T. The hardness of additively manufactured alloys. *Materials* **2018**, *11*, 2070. [CrossRef]
23. Dai, N.; Zhang, L.C.; Zhang, J.; Zhang, X.; Ni, Q.; Chen, Y.; Wu, M.; Yang, C. Distinction in corrosion resistance of selective laser melted Ti-6Al-4V alloy on different planes. *Corros. Sci.* **2016**, *111*, 703–710. [CrossRef]
24. Lin, J.; Lv, Y.; Liu, Y.; Sun, Z.; Wang, K.; Li, Z.; Wu, Y.; Xu, B. Microstructural evolution and mechanical property of Ti-6Al-4V wall deposited by continuous plasma arc additive manufacturing without post heat treatment. *J. Mech. Behav. Biomed. Mater.* **2017**, *69*, 19–29. [CrossRef]
25. Tamilselvi, S.; Raman, V.; Rajendran, N. Corrosion behaviour of Ti–6Al–7Nb and Ti–6Al–4V ELI alloys in the simulated body fluid solution by electrochemical impedance spectroscopy. *Electrochim. Acta* **2006**, *52*, 839–846. [CrossRef]
26. Castellanos, S.D.; Alves, J.L.; Neto, R.J. A comparative study of manufacturing processes of complex surface parts in Titanium Ti6Al4V. *Ciência Tecnol. Dos Mater.* **2017**, *29*, 73–78. [CrossRef]
27. Lütjering, G.; Williams, J.C. *Titanium*, 2nd ed.; Springer: New York, NY, USA, 2007. [CrossRef]
28. Huang, R.; Riddle, M.; Graziano, D.; Warren, J.; Das, S.; Nimbalkar, S.; Cresko, J.; Masanet, E. Energy and emissions saving potential of additive manufacturing: The case of lightweight aircraft components. *J. Clean. Prod.* **2016**, *135*, 1559–1570. [CrossRef]
29. Ngo, T.D.; Kashani, A.; Imbalzano, G.; Nguyen, K.T.Q.; Hui, D. Additive manufacturing (3D printing): A review of materials, methods, applications and challenges. *Compos. Part B Eng.* **2018**, *143*, 172–196. [CrossRef]
30. Ducato, A.; Fratini, L.; La Cascia, M.; Mazzola, G. An automated visual inspection system for the classification of the phases of Ti-6Al-4V titanium alloy. *Lect. Notes Comput.* **2013**, *8048*, 362–369. [CrossRef]
31. Ahmed, T.; Rack, H.J. Phase transformations during cooling in α+β titanium alloys. *Mater. Sci. Eng. A* **1998**, *243*, 206–211. [CrossRef]
32. Boyer, R.; Collings, E.W.; Welsch, G. *Materials Properties Handbook: Titanium Alloys*; ASM International: Cleveland, OH, USA, 1994.
33. Gil Mur, F.X.; Rodríguez, D.; Planell, J.A. Influence of tempering temperature and time on the α′-Ti-6Al-4V martensite. *J. Alloys Compd.* **1996**, *234*, 287–289. [CrossRef]
34. Reisgen, U.; Olschok, S.; Sharma, R.; Gach, S. Influence on martensite-start-temperature and volume expansion of low-transformation-temperature materials used for residual stress relief in beam welding. *Mater. Sci. Eng. Technol.* **2017**, *48*, 1276–1282. [CrossRef]
35. Liu, S.; Shin, Y.C. Additive manufacturing of Ti6Al4V alloy: A review. *Mater. Des.* **2019**, *164*, 107552. [CrossRef]
36. Bartlett, J.L.; Li, X. An overview of residual stresses in metal powder bed fusion. *Addit. Manuf.* **2019**, *27*, 131–149. [CrossRef]
37. Vayssette, B.; Saintier, N.; Brugger, C.; Elmay, M.; Pessard, E. Surface roughness of Ti-6Al-4V parts obtained by SLM and EBM: Effect on the High Cycle Fatigue life. *Procedia Eng.* **2018**, *213*, 89–97. [CrossRef]
38. Liu, D.; Flewitt, P.E.J. Raman measurements of stress in films and coatings. *Spectrosc. Prop. Inorg. Organomet. Compd.* **2014**, *45*, 141–177. [CrossRef]
39. Guo, J.; Fu, H.; Pan, B.; Kang, R. Recent progress of residual stress measurement methods: A review. *Chin. J. Aeronaut.* **2020**. [CrossRef]
40. Barros, R.; Silva, F.J.G.; Gouveia, R.M.; Saboori, A.; Marchese, G.; Biamino, S.; Salmi, A.; Atzeni, E. Laser Powder Bed Fusion of Inconel 718: Residual Stress Analysis Before and After Heat Treatment. *Metals* **2019**, *9*, 1290. [CrossRef]
41. ASTM E 837-08. *Standard Test Method for Determining Residual Stresses by the Hole-Drilling Strain-Gages*; ASTM International: West Conshohocken, PA, USA, 2008; Volume 1, pp. 1–17.
42. Thijs, L.; Verhaeghe, F.; Craeghs, T.; Humbeeck, J.V.; Kruth, J.P. A study of the microstructural evolution during selective laser melting of Ti-6Al-4V. *Acta Mater.* **2010**, *58*, 3303–3312. [CrossRef]
43. Facchini, L.; Magalini, E.; Robotti, P.; Molinari, A.; Höges, S.; Wissenbach, K. Ductility of a Ti-6Al-4V alloy produced by selective laser melting of prealloyed powders. *Rapid Prototyp. J.* **2010**, *16*, 450–459. [CrossRef]
44. Gong, H.; Rafi, K.; Gu, H.; Janaki Ram, G.D.; Starr, T.; Stucker, B. Influence of defects on mechanical properties of Ti-6Al-4V components produced by selective laser melting and electron beam melting. *Mater. Des.* **2015**, *86*, 545–554. [CrossRef]

45. Benedetti, M.; Torresani, E.; Leoni, M.; Fontanari, V.; Bandini, M.; Pederzolli, C.; Potrich, C. The effect of post-sintering treatments on the fatigue and biological behavior of Ti-6Al-4V ELI parts made by selective laser melting. *J. Mech. Behav. Biomed. Mater.* **2017**, *71*, 295–306. [CrossRef]
46. Xu, W.; Sun, S.; Elambasseril, J.; Liu, Q.; Brandt, M.; Qian, M. Ti-6Al-4V Additively Manufactured by Selective Laser Melting with Superior Mechanical Properties. *JOM* **2015**, *67*, 668–673. [CrossRef]
47. Xu, J.; Zhu, J.; Fan, J.; Zhou, Q.; Peng, Y.; Guo, S. Microstructure and mechanical properties of Ti–6Al–4V alloy fabricated using electron beam freeform fabrication. *Vacuum* **2019**, *167*, 364–373. [CrossRef]
48. Galarraga, H.; Lados, D.A.; Dehoff, R.R.; Kirka, M.M.; Nandwana, P. Effects of the microstructure and porosity on properties of Ti-6Al-4V ELI alloy fabricated by electron beam melting (EBM). *Addit. Manuf.* **2016**, *10*, 47–57. [CrossRef]
49. Zhao, X.; Li, S.; Zhang, M.; Liu, Y.; Sercombe, T.B.; Wang, S.; Hao, Y.; Yang, R.; Murr, L.E. Comparison of the microstructures and mechanical properties of Ti-6Al-4V fabricated by selective laser melting and electron beam melting. *Mater. Des.* **2016**, *95*, 21–31. [CrossRef]
50. Chern, A.H.; Nandwana, P.; McDaniels, R.; Dehoff, R.R.; Liaw, P.K.; Tryon, R.; Duty, C.E. Build orientation, surface roughness, and scan path influence on the microstructure, mechanical properties, and flexural fatigue behavior of Ti–6Al–4V fabricated by electron beam melting. *Mater. Sci. Eng. A* **2020**, *772*, 138740. [CrossRef]
51. Murr, L.E.; Esquivel, E.V.; Quinones, S.A.; Gaytan, S.M.; Lopez, M.I.; Martinez, E.Y.; Medina, F.; Hernandez, D.H.; Martinez, E.; Martinez, J.L.; et al. Microstructures and mechanical properties of electron beam-rapid manufactured Ti-6Al-4V biomedical prototypes compared to wrought Ti-6Al-4V. *Mater. Charact.* **2009**, *60*, 96–105. [CrossRef]
52. Edwards, P.; Ramulu, M. Fatigue performance evaluation of selective laser melted Ti-6Al-4V. *Mater. Sci. Eng. A* **2014**, *598*, 327–337. [CrossRef]
53. Chan, K.S.; Koike, M.; Mason, R.L.; Okabe, T. Fatigue life of titanium alloys fabricated by additive layer manufacturing techniques for dental implants. *Metall. Mater. Trans. A Phys. Metall. Mater. Sci.* **2013**, *44*, 1010–1022. [CrossRef]
54. Fousová, M.; Vojtěch, D.; Doubrava, K.; Daniel, M.; Lin, C.F. Influence of inherent surface and internal defects on mechanical properties of additively manufactured Ti6Al4V alloy: Comparison between selective laser melting and electron beam melting. *Materials* **2018**, *11*, 537. [CrossRef] [PubMed]
55. Qiu, C.; Panwisawas, C.; Ward, M.; Basoalto, H.C.; Brooks, J.W.; Attallah, M.M. On the role of melt flow into the surface structure and porosity development during selective laser melting. *Acta Mater.* **2015**, *96*, 72–79. [CrossRef]
56. Stef, J.; Poulon-Quintin, A.; Redjaimia, A.; Ghanbaja, J.; Ferry, O.; De Sousa, M.; Gouné, M. Mechanism of porosity formation and influence on mechanical properties in selective laser melting of Ti-6Al-4V parts. *Mater. Des.* **2018**, *156*, 480–493. [CrossRef]
57. Tammas-Williams, S.; Zhao, H.; Léonard, F.; Derguti, F.; Todd, I.; Prangnell, P.B. XCT analysis of the influence of melt strategies on defect population in Ti-6Al-4V components manufactured by Selective Electron Beam Melting. *Mater. Charact.* **2015**, *102*, 47–61. [CrossRef]
58. Ning, J.; Sievers, D.E.; Garmestani, H.; Liang, S.Y. Analytical modeling of part porosity in metal additive manufacturing. *Int. J. Mech. Sci.* **2020**, *172*, 105428. [CrossRef]
59. Zhang, W.; Qin, P.; Wang, Z.; Yang, C.; Kollo, L.; Grzesiak, D.; Prashanth, K.G. Superior wear resistance in EBM-Processed TC4 alloy compared with SLM and forged samples. *Materials* **2019**, *12*, 782. [CrossRef]
60. Mohammadhosseini, A.; Fraser, D.; Masood, S.H.; Jahedi, M. Microstructure and mechanical properties of Ti–6Al–4V manufactured by electron beam melting process. *Mater. Res. Innov.* **2013**, *17*, 106–112. [CrossRef]
61. Tan, X.; Kok, Y.; Tan, Y.J.; Descoins, M.; Mangelinck, D.; Tor, S.B.; Leong, K.F.; Chua, C.K. Graded microstructure and mechanical properties of additive manufactured Ti-6Al-4V via electron beam melting. *Acta Mater.* **2015**, *97*, 1–16. [CrossRef]
62. Losertová, M.; Kubeš, V. Microstructure and mechanical properties of selective laser melted Ti6Al4V alloy. *IOP Conf. Ser. Mater. Sci. Eng.* **2017**, *266*, 012009. [CrossRef]
63. Rafi, H.K.; Karthik, N.V.; Gong, H.; Starr, T.L.; Stucker, B.E. Microstructures and mechanical properties of Ti6Al4V parts fabricated by selective laser melting and electron beam melting. *J. Mater. Eng. Perform.* **2013**, *22*, 3872–3883. [CrossRef]

64. Balyakin, A.; Zhuchenko, E.; Nosova, E. Study of heat treatment impact on the surface defects appearance on samples obtained by selective laser melting of Ti-6Al-4V during chemical polishing. *Mater. Today Proc.* **2019**, *19*, 2307–2311. [CrossRef]
65. Vayssette, B.; Saintier, N.; Brugger, C.; El May, M. Surface roughness effect of SLM and EBM Ti-6Al-4V on multiaxial high cycle fatigue. *Theor. Appl. Fract. Mech.* **2020**, *108*, 102581. [CrossRef]
66. Yuan, W.; Hou, W.; Li, S.; Hao, Y.; Yang, R.; Zhang, L.C.; Zhu, Y. Heat treatment enhancing the compressive fatigue properties of open-cellular Ti-6Al-4V alloy prototypes fabricated by electron beam melting. *J. Mater. Sci. Technol.* **2018**, *34*, 1127–1131. [CrossRef]
67. Zhao, S.; Li, S.J.; Hou, W.T.; Hao, Y.L.; Yang, R.; Misra, R.D.K. The influence of cell morphology on the compressive fatigue behavior of Ti-6Al-4V meshes fabricated by electron beam melting. *J. Mech. Behav. Biomed. Mater.* **2016**, *59*, 251–264. [CrossRef]
68. Chastand, V.; Quaegebeur, P.; Maia, W.; Charkaluk, E. Comparative study of fatigue properties of Ti-6Al-4V specimens built by electron beam melting (EBM) and selective laser melting (SLM). *Mater. Charact.* **2018**, *143*, 76–81. [CrossRef]
69. Pegues, J.W.; Shao, S.; Shamsaei, N.; Sanaei, N.; Fatemi, A.; Warner, D.H.; Li, P.; Phan, N. Fatigue of additive manufactured Ti-6Al-4V, Part I: The effects of powder feedstock, manufacturing, and post-process conditions on the resulting microstructure and defects. *Int. J. Fatigue* **2020**, *132*, 105358. [CrossRef]
70. Molaei, R.; Fatemi, A.; Sanaei, N.; Pegues, J.; Shamsaei, N.; Shao, S.; Li, P.; Warner, D.H.; Phan, N. Fatigue of additive manufactured Ti-6Al-4V, Part II: The relationship between microstructure, material cyclic properties, and component performance. *Int. J. Fatigue* **2020**, *132*, 105363. [CrossRef]
71. Wu, M.-W.; Chen, J.-K.; Lin, B.-H.; Chiang, P.-H.; Tsai, M.-K. Compressive fatigue properties of additive-manufactured Ti-6Al-4V cellular material with different porosities. *Mater. Sci. Eng. A* **2020**, *790*, 139695. [CrossRef]
72. Viespoli, L.M.; Bressan, S.; Itoh, T.; Hiyoshi, N.; Prashanth, K.G.; Berto, F. Creep and high temperature fatigue performance of as build selective laser melted Ti-based 6Al-4V titanium alloy. *Eng. Fail. Anal.* **2020**, *111*, 104477. [CrossRef]
73. Yu, H.; Li, F.; Wang, Z.; Zeng, X. Fatigue performances of selective laser melted Ti-6Al-4V alloy: Influence of surface finishing, hot isostatic pressing and heat treatments. *Int. J. Fatigue* **2019**, *120*, 175–183. [CrossRef]
74. Kim, Y.K.; Park, S.H.; Yu, J.H.; AlMangour, B.; Lee, K.A. Improvement in the high-temperature creep properties via heat treatment of Ti-6Al-4V alloy manufactured by selective laser melting. *Mater. Sci. Eng. A* **2018**, *715*, 33–40. [CrossRef]
75. Hemmasian Ettefagh, A.; Zeng, C.; Guo, S.; Raush, J. Corrosion behavior of additively manufactured Ti-6Al-4V parts and the effect of post annealing. *Addit. Manuf.* **2019**, *28*, 252–258. [CrossRef]
76. Wang, M.; Wu, Y.; Lu, S.; Chen, T.; Zhao, Y.; Chen, H.; Tang, Z. Fabrication and characterization of selective laser melting printed Ti–6Al–4V alloys subjected to heat treatment for customized implants design. *Prog. Nat. Sci. Mater. Int.* **2016**, *26*, 671–677. [CrossRef]
77. Pazhanivel, B.; Sathiya, P.; Sozhan, G. Ultra-fine bimodal ($\alpha + \beta$) microstructure induced mechanical strength and corrosion resistance of Ti-6Al-4V alloy produced via laser powder bed fusion process. *Opt. Laser Technol.* **2020**, *125*, 106017. [CrossRef]
78. Leon, A.; Levy, G.K.; Ron, T.; Shirizly, A.; Aghion, E. The effect of hot isostatic pressure on the corrosion performance of Ti-6Al-4 V produced by an electron-beam melting additive manufacturing process. *Addit. Manuf.* **2020**, *33*, 101039. [CrossRef]
79. Sharma, A.; Oh, M.C.; Kim, J.T.; Srivastava, A.K.; Ahn, B. Investigation of electrochemical corrosion behavior of additive manufactured Ti–6Al–4V alloy for medical implants in different electrolytes. *J. Alloys Compd.* **2020**, *830*, 154620. [CrossRef]
80. Nalli, F.; Bottini, L.; Boschetto, A.; Cortese, L.; Veniali, F. Effect of industrial heat treatment and barrel finishing on the mechanical performance of Ti6AL4V processed by selective laser melting. *Appl. Sci.* **2020**, *10*, 2280. [CrossRef]
81. Wysocki, B.; Maj, P.; Sitek, R.; Buhagiar, J.; Kurzydłowski, K.J.; Świeszkowski, W. Laser and electron beam additive manufacturing methods of fabricating titanium bone implants. *Appl. Sci.* **2017**, *7*, 657. [CrossRef]
82. Zhai, Y.; Galarraga, H.; Lados, D.A. Microstructure, static properties, and fatigue crack growth mechanisms in Ti-6Al-4V fabricated by additive manufacturing: LENS and EBM. *Eng. Fail. Anal.* **2016**, *69*, 3–14. [CrossRef]

83. Vrancken, B.; Thijs, L.; Kruth, J.P.; Van Humbeeck, J. Heat treatment of Ti6Al4V produced by Selective Laser Melting: Microstructure and mechanical properties. *J. Alloys Compd.* **2012**, *541*, 177–185. [CrossRef]
84. Vilaro, T.; Colin, C.; Bartout, J.D. As-fabricated and heat-treated microstructures of the Ti-6Al-4V alloy processed by selective laser melting. *Metall. Mater. Trans. A Phys. Metall. Mater. Sci.* **2011**, *42*, 3190–3199. [CrossRef]
85. Koike, M.; Greer, P.; Owen, K.; Lilly, G.; Murr, L.E.; Gaytan, S.M.; Martinez, E.; Okabe, T. Evaluation of titanium alloys fabricated using rapid prototyping technologies-electron beam melting and laser beam melting. *Materials* **2011**, *4*, 1776–1792. [CrossRef]
86. ASTM F136-08. *Standard Specification for Wrought Titanium-6Aluminum-4Vanadium ELI (Extra Low Interstitial) Alloy for Surgical Implant Applications (UNS R56401)*; ASTM International: West Conshohocken, PA, USA, 2008. Available online: www.astm.org (accessed on 24 June 2020).
87. Edwards, P.; O'Conner, A.; Ramulu, M. Electron Beam Additive Manufacturing of Titanium Components: Properties and Performance. *J. Manuf. Sci. Eng.* **2013**, *135*, 061016. [CrossRef]
88. Hayes, B.J.; Martin, B.W.; Welk, B.; Kuhr, S.J.; Ales, T.K.; Brice, D.A.; Ghamarian, I.; Baker, A.H.; Haden, C.V.; Harlow, D.G.; et al. Predicting tensile properties of Ti-6Al-4V produced via directed energy deposition. *Acta Mater.* **2017**, *133*, 120–133. [CrossRef]
89. Benzing, J.; Hrabe, N.; Quinn, T.; White, R.; Rentz, R.; Ahlfors, M. Hot isostatic pressing (HIP) to achieve isotropic microstructure and retain as-built strength in an additive manufacturing titanium alloy (Ti-6Al-4V). *Mater. Lett.* **2019**, *257*, 126690. [CrossRef]
90. Kasperovich, G.; Hausmann, J. Improvement of fatigue resistance and ductility of TiAl6V4 processed by selective laser melting. *J. Mater. Process. Technol.* **2015**, *220*, 202–214. [CrossRef]
91. Leuders, S.; Thöne, M.; Riemer, A.; Niendorf, T.; Tröster, T.; Richard, H.A.; Maier, H.J. On the mechanical behaviour of titanium alloy TiAl6V4 manufactured by selective laser melting: Fatigue resistance and crack growth performance. *Int. J. Fatigue* **2013**, *48*, 300–307. [CrossRef]
92. Simonelli, M.; Tse, Y.Y.; Tuck, C. Effect of the build orientation on the mechanical properties and fracture modes of SLM Ti-6Al-4V. *Mater. Sci. Eng. A* **2014**, *616*, 1–11. [CrossRef]
93. Galati, M.; Saboori, A.; Biamino, S.; Calignano, F.; Lombardi, M.; Marchiandi, G.; Minetola, P.; Fino, P.; Iuliano, L. Ti-6Al-4V lattice structures produced by EBM: Heat treatment and mechanical properties. *Procedia CIRP* **2020**, *88*, 411–416. [CrossRef]
94. Morita, T.; Tsuda, C.; Nakano, T. Influences of scanning speed and short-time heat treatment on fundamental properties of Ti-6Al-4V alloy produced by EBM method. *Mater. Sci. Eng. A* **2017**, *704*, 246–251. [CrossRef]
95. Zhang, X.Y.; Fang, G.; Leeflang, S.; Böttger, A.J.; Zadpoor, A.A.; Zhou, J. Effect of subtransus heat treatment on the microstructure and mechanical properties of additively manufactured Ti-6Al-4V alloy. *J. Alloys Compd.* **2018**, *735*, 1562–1575. [CrossRef]
96. Sabban, R.; Bahl, S.; Chatterjee, K.; Suwas, S. Globularization using heat treatment in additively manufactured Ti-6Al-4V for high strength and toughness. *Acta Mater.* **2019**, *162*, 239–254. [CrossRef]
97. Tsai, M.T.; Chen, Y.W.; Chao, C.Y.; Jang, J.S.C.; Tsai, C.C.; Su, Y.L.; Kuo, C.N. Heat-treatment effects on mechanical properties and microstructure evolution of Ti-6Al-4V alloy fabricated by laser powder bed fusion. *J. Alloys Compd.* **2020**, *816*, 152615. [CrossRef]
98. Galarraga, H.; Warren, R.J.; Lados, D.A.; Dehoff, R.R.; Kirka, M.M.; Nandwana, P. Effects of heat treatments on microstructure and properties of Ti-6Al-4V ELI alloy fabricated by electron beam melting (EBM). *Mater. Sci. Eng. A* **2017**, *685*, 417–428. [CrossRef]
99. Zhang, D.; Wang, L.; Zhang, H.; Maldar, A.; Zhu, G.; Chen, W.; Park, J.S.; Wang, J.; Zeng, X. Effect of heat treatment on the tensile behavior of selective laser melted Ti-6Al-4V by in situ X-ray characterization. *Acta Mater.* **2020**, *189*, 93–104. [CrossRef]
100. Ter Haar, G.M.; Becker, T.H. Selective laser melting produced Ti-6Al-4V: Post-process heat treatments to achieve superior tensile properties. *Materials* **2018**, *11*, 146. [CrossRef]
101. Mercelis, P.; Kruth, J.P. Residual stresses in selective laser sintering and selective laser melting. *Rapid Prototyp. J.* **2006**, *12*, 254–265. [CrossRef]
102. Kruth, J.P.; Deckers, J.; Yasa, E.; Wauthlé, R. Assessing and comparing influencing factors of residual stresses in selective laser melting using a novel analysis method. *Proc. Inst. Mech. Eng. Part B J. Eng. Manuf.* **2012**, *226*, 980–991. [CrossRef]

103. Zaeh, M.F.; Branner, G. Investigations on residual stresses and deformations in selective laser melting. *Prod. Eng.* **2010**, *4*, 35–45. [CrossRef]
104. Ali, H.; Ghadbeigi, H.; Mumtaz, K. Effect of scanning strategies on residual stress and mechanical properties of Selective Laser Melted Ti6Al4V. *Mater. Sci. Eng. A* **2018**, *712*, 175–187. [CrossRef]
105. Song, J.; Wu, W.; Zhang, L.; He, B.; Lu, L.; Ni, X.; Long, Q.; Zhu, G. Role of scanning strategy on residual stress distribution in Ti-6Al-4V alloy prepared by selective laser melting. *Optik* **2018**, *170*, 342–352. [CrossRef]
106. Lu, Y.; Wu, S.; Gan, Y.; Huang, T.; Yang, C.; Junjie, L.; Lin, J. Study on the microstructure, mechanical property and residual stress of SLM Inconel-718 alloy manufactured by differing island scanning strategy. *Opt. Laser Technol.* **2015**, *75*, 197–206. [CrossRef]
107. Maawad, E.; Sano, Y.; Wagner, L.; Brokmeier, H.G.; Genzel, C. Investigation of laser shock peening effects on residual stress state and fatigue performance of titanium alloys. *Mater. Sci. Eng. A* **2012**, *536*, 82–91. [CrossRef]
108. Tong, Z.; Ren, X.; Ren, Y.; Dai, F.; Ye, Y.; Zhou, W.; Chen, L.; Ye, Z. Effect of laser shock peening on microstructure and hot corrosion of TC11 alloy. *Surf. Coat. Technol.* **2018**, *335*, 32–40. [CrossRef]
109. Huang, S.; Zhu, Y.; Guo, W.; Peng, P.; Diao, X. Impact toughness and microstructural response of Ti-17 titanium alloy subjected to laser shock peening. *Surf. Coat. Technol.* **2017**, *327*, 32–41. [CrossRef]
110. Zhang, X.C.; Zhang, Y.K.; Lu, J.Z.; Xuan, F.Z.; Wang, Z.D.; Tu, S.T. Improvement of fatigue life of Ti-6Al-4V alloy by laser shock peening. *Mater. Sci. Eng. A* **2010**, *527*, 3411–3415. [CrossRef]
111. Ren, X.D.; Zhou, W.F.; Liu, F.F.; Ren, Y.P.; Yuan, S.Q.; Ren, N.F.; Xu, S.D.; Yang, T. Microstructure evolution and grain refinement of Ti-6Al-4V alloy by laser shock processing. *Appl. Surf. Sci.* **2016**, *363*, 44–49. [CrossRef]
112. Guo, W.; Sun, R.; Song, B.; Zhu, Y.; Li, F.; Che, Z.; Li, B.; Guo, C.; Liu, L.; Peng, P. Laser shock peening of laser additive manufactured Ti6Al4V titanium alloy. *Surf. Coat. Technol.* **2018**, *349*, 503–510. [CrossRef]
113. Jin, X.; Lan, L.; Gao, S.; He, B.; Rong, Y. Effects of laser shock peening on microstructure and fatigue behavior of Ti–6Al–4V alloy fabricated via electron beam melting. *Mater. Sci. Eng. A* **2020**, *780*, 139199. [CrossRef]
114. Lan, L.; Jin, X.; Gao, S.; He, B.; Rong, Y. Microstructural evolution and stress state related to mechanical properties of electron beam melted Ti-6Al-4V alloy modified by laser shock peening. *J. Mater. Sci. Technol.* **2020**, *50*, 153–161. [CrossRef]
115. Eyzat, Y.; Chemkhi, M.; Portella, Q.; Gardan, J.; Remond, J.; Retraint, D. Characterization and mechanical properties of As-Built SLM Ti-6Al-4V subjected to surface mechanical post-treatment. *Procedia CIRP* **2019**, *81*, 1225–1229. [CrossRef]
116. Yakout, M.; Elbestawi, M.A.; Veldhuis, S.C. A study of the relationship between thermal expansion and residual stresses in selective laser melting of Ti-6Al-4V. *J. Manuf. Process.* **2020**, *52*, 181–192. [CrossRef]
117. Vastola, G.; Zhang, G.; Pei, Q.X.; Zhang, Y.W. Controlling of residual stress in additive manufacturing of Ti6Al4V by finite element modeling. *Addit. Manuf.* **2016**, *12*, 231–239. [CrossRef]
118. Ning, J.; Praniewicz, M.; Wang, W.; Dobbs, J.R.; Liang, S.Y. Analytical modeling of part distortion in metal additive manufacturing. *Int. J. Adv. Manuf. Technol.* **2020**, *107*, 49–57. [CrossRef]